Fluidization of wet granulates under shear

S. H. Ebrahimnazhad Rahbari, J. Vollmer, S. Herminghaus, and M. Brinkmann
Department for Dynamics of Complex Fluids, Max-Planck Institute for Dynamics and Self-Organization, 37073 Göttingen, Germany
(Received 17 December 2009; revised manuscript received 6 October 2010; published 16 December 2010)

Small amounts of a wetting liquid render sand a stiff and moldable material. The cohesive forces between the sand grains are caused by capillary bridges at the points of contact. Due to the finite strength of these bridges wet sand undergoes a transition from an arrested (i.e., solidified) to a fluidized state under an externally applied shear force. The transition between these two dynamic states is studied in a MD-type simulation of a two-dimensional assembly of bidisperse frictionless disks under the action of a cosine force profile. In addition to soft core repulsion the disks interact through a hysteretic and short ranged attractive force modeling the effect of the capillary bridges. In this model the transition between the fluidized and the arrested state is discontinuous and hysteretic. The parameter dependence of the critical force for solidification is modeled by combining theoretical arguments with a detailed numerical exploration of the transition. We address a range of densities from slightly below close packing until slightly above densities where the system approaches a shear-banded state. Differences and similarities of the transition in wet granulates to the jamming transition are also addressed.

DOI: 10.1103/PhysRevE.82.061305 PACS number(s): 45.70.−n, 62.20.M−, 45.05.+x

I. INTRODUCTION

Dry sand behaves very much like a fluid, as it tends to make a horizontal interface to the space above, or runs easily through the orifice of an hourglass [1–6]. This changes drastically when the sand becomes wet, as can be judged from the pasty material from which sand castles are sculpted at the beach [7]. This is due to liquid capillary bridges extending between neighboring grains at their mutual points of contact, which exert an attractive force by virtue of the surface tension of the liquid [7–9]. A wet granulate thus exhibits both cohesion and stiffness, and is able to withstand a certain shear stress without yielding. As a critical value of applied stress is reached, however, the material starts to flow plastically [10]. This transition and its corresponding yield stress is of great importance for phenomena as diverse as land slides in unsaturated soils or agglomeration and kneading processes in food and pharmaceutical industry. Similar to the jamming transition of dry granular packings [11–16], the shear-induced fluidization of wet granulates exhibits many features analogous to a phase transition, although dominated microscopically by dissipative processes [17]. This suggests wet granular matter as another model system for the study of phase transitions far from thermal equilibrium [18–20].

In the present paper, we present numerical simulation and theoretical arguments addressing the transition from a fluidized to an arrested state [41] in a model wet granulate under applied shear forces. The setting is chosen similar to a previous study [17], in which a three-dimensional (3D) packing of spheres was subject to a body force field varying harmonically in space. In search for the simplest possible model capturing the influence of a wetting liquid, the capillary bridges between adjacent spheres are modeled by a hysteretic, piecewise-constant attractive force (minimal capillary model). The overall liquid content of the granular pile manifests itself in this model in the rupture separation of a capillary bridge, i.e., in its maximal extension, which is a monotonously growing function of the liquid volume.

It was found [17,21,22] that the so defined wet granular pile resisted the applied shear field up to a certain threshold, above which a large-scale particle flow set in. Thus, the existence of a finite yield stress was successfully captured. Remarkably [17], the average power of the fluctuations diverged algebraically as the threshold was approached, and above the threshold, both the diffusivity and the average drift velocity increased with increasing force according to a simple power law. This was rationalized by simple considerations of the network of capillary bridges and their rupture frequency [8]. Behavior very much reminiscent to critical phenomena has also been reported for the arrest of flow in granular packings with purely repulsive interactions [12–16]. In the latter context the arrested state is called a *jammed* state, and it was asserted that the transition solely depends on two control parameters: density and external shear. Moreover, the comparison of thermal energies to the strength of particle interactions constitutes a third control parameter [11,12,23–26].

In the present work we discuss extensive numerical simulations with a particular focus on a systematic variation of model parameters. In this way, we are able to distinguish universal and nonuniversal aspects of the fluidization transition of wet granulates under shear, and we map out the phase diagram spanned by liquid content, external forcing, and packing density. Theoretical arguments disclose the dependence of the force for fluidization and arrest of the system on these parameters.

For the sake of numerical efficiency the present study only addresses the two-dimensional (2D) case. A systematic comparison of systems with different dimensionality is left to forthcoming studies.

The paper is organized as follows: in Sec. II we recapitulate some basic features about capillary forces, introduce the model for the wet granulate, its numerical implementation, and details of the protocols used to generate dense assemblies of disks. In Sec. III we show the results of simulations of two-dimensional sheared assemblies of frictionless wet disks. The shearing motion is induced through coupling the

disks to a spatially heterogeneous external force. In the simulations the overall density of disks is fixed unlike simulations of granular piles on an inclined plane or in a rotating drum where the particles have sufficient space to adopt a preferred packing density. The simulations provide us with a dynamic phase diagram for the parameter dependence of the critical forces where the assembly of disks fluidizes and solidifies. The main trends of the solidification can be understood based on theoretical considerations. Finally, we conclude in Sec. IV At that point we also address similarities and differences to the corresponding transitions of dry granulates and of particles with attractive interactions.

II. MODEL

The main features of wet granular matter can be traced down to the cohesive forces exerted by liquid capillary bridges [7–9,27–29], which appear as toroidal structures located at the mechanical contacts of neighboring grains. The most important aspect of this attractive interaction is its hysteretic nature [8,9]. This corresponds to the fact that the formation of a capillary bridge needs two grains to come into contact, while the bridge can persist up to a certain separation of the grain surfaces. This observation inspires the use of hysteretic two-body interactions to account for cohesive capillary forces, at least in the range of low liquid saturations [8,18–20] on which we will focus here.

The phase diagram of wet granular matter under vertical vibration has been recently shown to be remarkably resistant to variations of the interaction force characteristics [30]. To a very good approximation the collective behavior of the grains is described in that case by only two dimensionless parameters: the shaking amplitude measured in units of the particle diameter, and the shaking frequency measured in units of particle mass, particle size, and the total energy lost upon the formation and rupture of a capillary bridge [19,30]. This can be taken as a justification to disregard details of the (experimentally known) force-distance characteristics of wet grain contacts, for the sake of both simulation efficiency and focus of physical insight.

In the present study of wet granular matter, we thus employ the minimal capillary model as before [8,17,30]. Owing to its simplicity, this model is well suited to perform numerical simulations of dense systems, involving a large number of particles [18,19,30]. An essential feature of capillary forces which is faithfully captured in this model is the role of the history of inter-particle separation. In order to be able to perform computations with large systems and to perform finite-size-scaling studies, we restrict our investigations here to the two-dimensional case. The system under consideration consists of a two-dimensional packing of circular disks subject to an external in-plane force field and binary interactions accounting for hard-core repulsion and capillary interactions.

A. Interactions

Capillary interactions are modeled as a force which arises instantaneously once two particles touch each other, and which acts as long as the separation, s, between their surfaces does not exceed a critical length s_c. In other words, the capillary bridge ruptures exactly at that moment when the particle separation s first exceeds the value of s_c. For the sake of simplicity, the attractive capillary bridge force, F_c, is assumed to be independent of disk separation s, and identical for all pairs of disks.

In contrast to restitution models used to study the dynamics of dry granulates [6], a *fixed* amount of energy

$$\varepsilon \equiv \int_0^{s_c} F_c \, ds = F_c \, s_c \tag{1}$$

is dissipated at each collision. For capillary bridges between spherical particles the rupture distance s_c of the a capillary bridge can be linked to the volume of the liquid bridges, e.g., by the formula given by Willet in Ref. [27]. In the remainder of this paper, the capillary force F_c will be used as a force scale. According to Eq. (1) the rupture energy ε is then the only free parameter determining the effect of capillary bridges.

We use a 1:1 mixture of large and small disks of respective radii R_l and R_s with a ratio $R_l/R_s=1.4$. This choice prevents the assembly to build up a long-range crystalline order [12]. Assuming a constant mass per area, ρ, the individual mass of disk i is $m_i=\pi\rho R_i^2$. Mutual repulsion between the disks is modeled by a soft-core nonlinear spring giving rise to a repulsive force

$$F_r(r_{ij}) = \begin{cases} C_{ij}\,(R_i + R_j - r_{ij})^{1/2} & \text{for } r_{ij} \le R_i + R_j \\ 0 & \text{else,} \end{cases} , \tag{2a}$$

where r_{ij} is the Euclidean distance between the center of disk i and j. In the spirit of Hertz's contact law [6] we set

$$C_{ij} = C\left(\frac{R_i R_j}{R_i + R_j}\right)^{1/2} \tag{2b}$$

in order to account for different disk radii. The global parameter C controls the hardness of the disks.

The disks are exposed to a spatially heterogeneous external force field of the form (cf. Fig. 1, top)

$$\mathbf{F}_{ex}(\mathbf{r}) = \mathbf{e}_y F_e \cos\left(\frac{2\pi x}{\lambda}\right), \tag{3}$$

where $\mathbf{r}=(x,y)$ is the position, $\mathbf{e}_y$ the unit vector pointing into y direction, F_e the amplitude of the external force, and λ the wavelength of the spatial modulation. The external field pulls the disks upward close to $x=0$ and $x=L$, and it pushes them downward close to $x=L/2$. There is no net force on a spatially uniform system such that the center of mass of all disks remains fixed in space except for a small noise due to deviations of the particle distribution from a uniform state.

Altogether, Newton's equation of motion for disk i reads

$$m_i \frac{d^2\mathbf{r}_i}{dt^2} = \mathbf{F}_{ex}(\mathbf{r}_i) - \sum_{j\in\mathcal{N}(i)} \mathbf{e}_{ij} f_{ij}(r_{ij}), \tag{4}$$

where m_i and $\mathbf{r}_i$ are the mass and the position of disk i, respectively, $\mathcal{N}(i)$ is the set of neighbors j interacting with i, the unit vector $\mathbf{e}_{ij}$ points from the center of disk i to the center of disk j, and f_{ij} is the force exerted by disk i on disk

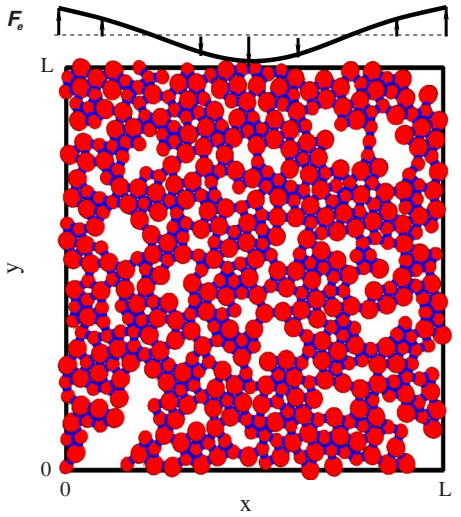

FIG. 1. (Color online) Sketch of the applied external force profile (top) together with a snapshot of an solidified arrangement of disks at time $t=1500$ when applying an external force of amplitude $F_e=4.5\times10^{-3}$. Simulations are performed in a square box with periodic boundary conditions. The area fraction of the disks is $\phi=0.7$, the rupture energy $\varepsilon=0.01$, and the box size is $L=\lambda=18$.

j. The latter force comprises the soft-core repulsion Eq. (2), and, whenever applicable, also the attractive force F_c modeling capillary bridges.

Throughout the remainder of this paper, we employ dimensionless rescaled quantities based on the capillary force F_c, the area mass density of the disks ρ, and the average disk diameter D. Time t and mass m is hence measured in units $\tau\equiv\sqrt{\rho D^3/F_c}$, and $\mu\equiv\rho D^2$, respectively. Using these normalized quantities it is straightforward to normalize all physical quantities derived from mass, length, and time, such as the local averages of disk velocities and the shear rate.

B. Boundary conditions and numerical implementation

In the simulations the wavelength λ of the force profile agrees with the lateral dimensions L of the square simulation box ranging between $18D$ and $120D$. Periodic boundary conditions are applied in both directions. The area fraction of disks, $\phi=A_d/L^2$, where A_d is the total area of the disks, varies between 0.52 and 0.85. The rescaled hardness parameter of the particles is set to $C=10^2$ throughout the simulations.

Dense assemblies of disks are obtained by a method similar to the algorithm proposed by Lubachevsky and Stillinger in Ref. [31]. However, instead of thermostating the system to a constant total kinetic energy, a viscous drag force

$$\mathbf{F}_{\text{drag}}=-b\mathbf{v}_i \tag{5}$$

acting on each disk i with velocity $\mathbf{v}_i$ dissipates the work that the system receives while inflating the disks.

Newton's equations of motion are integrated by means of a fifth order predictor-corrector scheme (also known as Gear's algorithm, see, e.g., [6]). The computation of forces between neighboring particles is speeded up by keeping local lists of disks residing in bins of a square array of cells. These bins are also used to compute and store local averages of the velocity and the number densities of small and large disks. In addition to the local averages taken over all disks in a bin, we time averaged these quantities over a certain period Δt. A further average over all bins in a column into y direction can be taken in a stationary flow field where the averaged velocity does not depend on the y coordinate.

C. Sample preparation

We use two different protocols to prepare initial disk configurations. Both protocols start with the inflation of initially very small particles. During this period energy is removed from the system by a viscous drag force. The external force and the capillary force are still set to zero.

In protocol (I) both the external force and the capillary forces are switched on simultaneously when having reached the desired packing fraction.

In protocol (II) the inflation of particles is followed by a tempering during a period $\Delta t=200$ where the capillary interaction is switched on while the drag force is still acting. Subsequently, during the actual simulation period the drag force is switched off and the external driving force Eq. (3) is switched on.

III. RESULTS

We performed extensive simulations for different area fractions ϕ and rupture energy ε. During a simulation run the amplitude of the external force F_e, was either fixed, or slowly ramped up and down to explore the history dependence of the dynamic states.

A. Velocity and shear profiles

For $\phi>0.52$ the flow field always approaches a stationary state, where to a very good approximation the density remains spatially uniform. An example is shown in Fig. 1.

For small external forces the systems approach an arrested state, while for sufficiently large external forces the system attains a velocity profile $v_y(x)$ along the external field with some superimposed velocity fluctuations. For sake of suppressing fluctuations and attaining a reasonable statistics the profiles will always be calculated by averaging along the columns where the external force takes constant values. The cosine-like functions in Fig. 2 (left axis) show the resulting velocity profiles for $F_e=1.32\times10^{-2}$ and $F_e=6.6\times10^{-3}$, respectively.

Velocity profiles tend to be flatter than the cosine close to the extrema of $F_{ex}(x)$, and steeper in between, as can clearly be seen from the profiles of the shear rate $\dot{\gamma}=\partial_x v_y(x)$, which is also displayed in Fig. 2 (right axis).

This trend, which is more enhanced when approaching the solidification transition, may be attributed to the fact that the fluidization is mainly due to the shear gradients close to the zeros of the force profile, while the disks tend to arrest close to force extrema.

In line with this the velocity profile takes its extreme values at $x\simeq L/4$ and $x\simeq 3L/4$ where the shear stresses are maximal. The difference

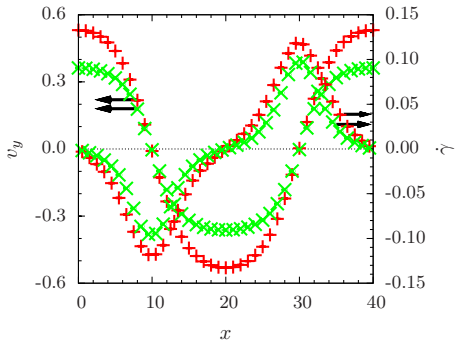

FIG. 2. (Color online) Profiles for the velocity component v_y parallel to the applied external field (curves indicated by arrows pointing to the left scale) and the shear rate $\dot{\gamma} \equiv \partial_x v_y$ (curves indicated by arrows pointing to right scale) in the steady state of systems with $F_e = 1.32 \times 10^{-2}$ (red +) and $F_e = 6.6 \times 10^{-3}$ (green ×), respectively. The area fraction of the disks is $\phi = 0.7$, the rupture energy $\varepsilon = 0.01$, and $L = 40$.

$$\Delta v_y = \frac{1}{2}[v_y(x=0) - v_y(x=L/2)] \tag{6}$$

of these extreme values takes on a zero or small value when the entire assembly of disks behaves like a rigid object, i.e., for arrested particle configurations. On the other hand, a nonzero value of Δv_y implies that the assembly is in a fluidized state.

The transition from the solidified to the fluidized state (and vice versa) can hence conveniently be monitored by adopting the difference Eq. (6) as an order parameter.

B. Approach toward a steady state

In Fig. 3 we show the time evolution of the order parameter after switching on the external force in protocol (I). The

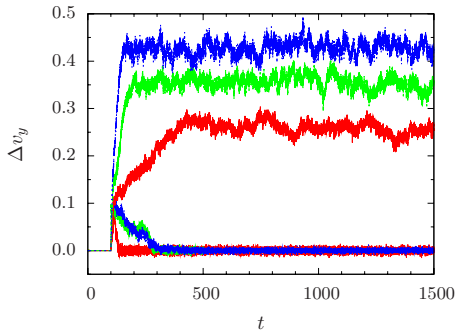

FIG. 3. (Color online) Order parameter Δv_y of the fluidization transition as function of time t for different amplitudes of the external force $F_e = 4.5 \times 10^{-3}$, 8×10^{-3}, 8.5×10^{-3}, 9×10^{-3}, 1.3×10^{-2}, 1.8×10^{-2} from bottom to top, respectively. After a certain relaxation time the system reaches a stationary state. For the three smallest values of the force the disk assembly reaches a solidified state where $\Delta v_y \equiv 0$, and for larger forces the system approaches a fluidized state where Δv_y takes positive values that increase upon increasing F_e. The area fraction of the disks is $\phi = 0.7$, the rupture energy $\varepsilon = 0.01$, and $L = 18$. The disk assembly shown in Fig. 1 amounts to the final configuration of the smallest force shown here.

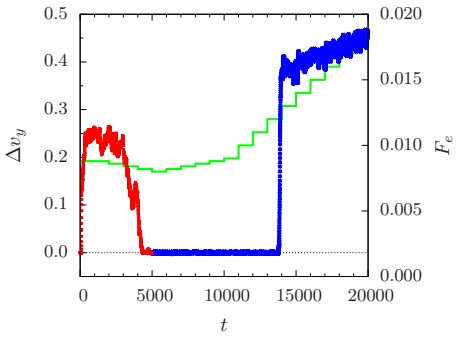

FIG. 4. (Color online) The red ($t < 5000$) and blue ($t > 5000$) curve shows the order parameter Δv_y as function of time during a stepwise change of the amplitude of the external force F_e (thin green line). The total area fraction of the disks is $\phi = 0.7$, the rupture energy $\varepsilon = 0.01$, and the system size $L = 18$. The zero line of the order parameter is indicated by a dotted line.

assembly of disks approaches a solidified state if the amplitude of the external driving F_e is smaller than $F_s \simeq 8.7 \times 10^{-3}$. In the solidified state the relative position of the disks in the assembly remains fixed.

Naturally, there are small fluctuations of the relative position of the disks, and the center-of-mass velocity in y direction might increase linearly due to a nonzero net force acting on the center of mass of a spatially inhomogeneous disk assembly.

For $F_e \gtrsim F_s$ the assembly of disks behaves like a fluid phase. On average, the disks follow the direction of the applied field while their local coordination shell of neighboring disks changes all the time.

The occurrence of these different types of asymptotic behavior can be explained by the nature of the initial state in the ensemble method (I). Due to the preparation the system is found in a fluidized state at the beginning of the simulation. Depending on the magnitude of the driving force, the system may stay permanently fluidized (for $F \gtrsim F_s$) or the fluidized state may only be a transient state (for $F \lesssim F_s$).

C. Fluidization and solidification transitions

The solidification and fluidization of a sheared granular system is explored by following the evolution while slowly changing the strength of the forcing in small steps (solid line in Fig. 4).

The simulation is started at a high driving strength $F_e \gg F_s$ such that the disks are initially in a fluidized state. Subsequently, the external force F_e is decreased. The red curve in Fig. 4 shows the corresponding values of the order parameter Δv_y. Its sharp drop at $t \simeq 4500$ clearly marks the solidification of the assembly of disks.

Comparison to Fig. 3 reveals that this transition occurs at exactly that value of the external force F_s, which also separates initial conditions approaching a fluidized state from those decaying to an arrested state for initial conditions prepared according to protocol (I). Solidification is encountered at the force F_s which does not dependent on the initial preparation protocol. It is determined only by the system size L, the packing fraction ϕ and the rupture energy ε.

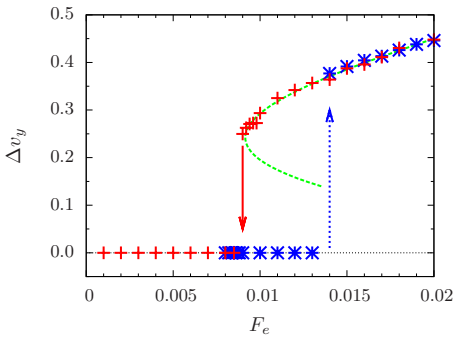

FIG. 5. (Color online) The red crosses (+) and blue stars (*) show the average values of the order parameter Δv_y evaluated over the time intervals of constant forcing in a simulation as shown in Fig. 4. The crosses refer to the values obtained while decreasing the external force from a fluidized state (F_e=0.02) to a point where the system is far in the region of solidified states. The stars show the values of the order parameter while F_e is increased until the system returns to the fluidized state. The dotted green line is a fit with a third order polynomial in the order parameter.

After solidification, the assembly shows thermal motion in a frozen network of capillary bridges ($5000 \lesssim t \lesssim 13\,000$ in Fig. 3). This motion persists since energy is preserved as long as no capillary bridges rupture.

When slowly increasing the external force stress is built up in the solidified state. Eventually it leads to a transition toward a fluidized state, when the applied external force exceeds a critical force F_f.

The force required for fluidization depends on the thermal energy remaining in the system when it is frozen. To avoid this dependence on the sample history one can remove the thermal motion by applying a viscous drag force [Eq. (5)] before increasing the external shear force. However, even in that case different solidified states require noticeably different critical forces F_f for fluidization: the critical force F_f required to fluidize the solidified state depends on details of the frozen network of capillary bridges. In contrast to F_s the force F_f is not a function of merely the system size L, the packing fraction ϕ and the rupture energy ε.

According to Fig. 4 the transition between the fluidized and solidified state is subjected to substantial hysteresis. The nature of this transition becomes clear when plotting the order parameter in its dependence on the external forcing F_e (cf. Fig. 5). For the particular parameters of the system there is a discontinuous jump in the order parameter as the control parameter is decreased across $F_s \simeq 0.0087$, where the system freezes into a solidified state. Similarly, a discontinuous jump in the order parameter from zero to a finite value occurs during an increase of the external force beyond $F_f \simeq 0.013$ where the system returns to the fluidized state. The hysteresis in the curve and the shape of the order parameter in the fluidized state indicate that the fluidized state arises by a saddle-node bifurcation, and the arrested state looses stability in a subcritical bifurcation.

D. System-size dependence of critical forces

To gain insight into the solidification transition, we consider a very slow creeping flow $v_y(x)$ at the edge of arrest. The input power that is injected by means of the external force acting on the disks is given by

$$\langle P_{\text{forcing}} \rangle = \int_0^L dx \; v_y(x)\, F_{\text{ex}}(x)\, n(x), \tag{7}$$

where $F_{\text{ex}}(x)$ is local y component of the external force and $n(x)$ the number of particles per unit length dx (i.e., the number of particles in a rectangle of size $L \times dx$ aligned parallel to the external field). As pointed out in Sec. III A the density may be regarded as uniform in the simulation box such that $n(x)$ takes the constant value N/L where N denotes the number of disks.

Assuming that the velocity profile is faithfully approximated by its first even harmonic, i.e., $v_y(x) \simeq \Delta v_y \cos(2\pi x/L)$, we obtain the estimate

$$\langle P_{\text{forcing}} \rangle \simeq N \frac{\Delta v_y F_e}{2} \tag{8}$$

for the injected power. On the other hand, the velocity profiles found in our simulations (cf. Fig. 2) show noticeable deviations from the fundamental harmonic. Especially when the external force is close to the solidification point there is a tendency to be flattened around the extrema. However, this deviation has no strong influence on the estimate Eq. (8), as one verifies by considering the extreme case of a plug flow, $v_y(x) \simeq \Delta v_y \, \text{sign}(F_{\text{ex}}(x))$, of two bands with arrested particle configuration separated by a thin shear band. This velocity profile yields the estimate

$$\langle P_{\text{forcing}} \rangle \simeq N \frac{2\Delta v_y F_e}{\pi}, \tag{9}$$

which differs only by a factor $\pi/4$ from Eq. (8).

In order to calculate the power dissipated by rupturing of capillary bridges, we observe that for each disk the creeping flow enforces a change of neighbors (in the direction of the flow) with a rate $\dot{\gamma} = dv_y/dx$. If ν denotes the average number of capillary bridges which break on a disk until $\gamma = 1$, such a displacement goes along with an energy dissipation $\nu\varepsilon$. The total dissipated power is thus given by

$$\langle P_{\text{diss}} \rangle = \int_0^L dx \; n(x) \left| \frac{dv_y}{dx} \right| \nu\varepsilon. \tag{10}$$

For every function $v_y(x)$ with period L this integral yields

$$\langle P_{\text{diss}} \rangle \simeq N \frac{4\nu\varepsilon\Delta v_y}{L}, \tag{11}$$

where again we used that the particle density is spatially uniform, $n(x) \equiv N/L$.

In a steady state, the input power $\langle P_{\text{forcing}} \rangle$ is balanced by the dissipated power $\langle P_{\text{diss}} \rangle$, so that we obtain the following estimate for the minimum forcing required to maintain the flow

$$F_s \simeq \frac{8\nu\varepsilon}{L}, \tag{12}$$

provided that the velocity profile is close to the fundamental harmonic. For the rather extreme opposite case of a plug

flow, the estimate Eq. (12) for F_s is multiplied by a factor of $\pi/4$.

To also gain some insight into the fluidization transition we note that the system is subjected to a body force acting in upward and downward direction in the regions $[0,L/2]$ and $[L/2,L]$, respectively. Due to the propagation of forces in the wet granular packing [21] these forces give rise to a stress of the order of $\sigma \simeq NF_e/L$ at the inflection point of the force profile. This stress has to be counterbalanced by $\nu NR/L$ capillary bridges in that region such that $\sigma L \sim \nu NR/L$. Relating the stress, NF_f/L, at the fluidization threshold, where the system yields, with the maximum force carried by the capillary bridges in that region, $F_c \nu NR/L$, and measuring forces and length scales in units of F_c and R, respectively, one again finds

$$F_f \sim \frac{\nu}{L}. \tag{13}$$

Equation (12) expresses an inverse linear scaling of F_s with the lateral extension L of the system. This can be interpreted as follows: in the fluidized state the shear rate takes a fairly sharp maximum in the region where the external force has its turning point (cf. Fig. 2) such that an energy input in the bulk is counterbalanced by dissipation in a localized region. The system is arrested when the capillary bridges located close to the turning points of the force profile are sufficiently strong to suppress the relative motion of the parts of the system which are pushed upward and downward, respectively. Similarly, the analogous scaling in Eq. (13) arises from the fact that the strain introduced in the system by a body force has to be counteracted by capillary bridges in a region close to the inflection point of the external force. In both cases the scaling hence comes down to stating that the respective critical force is related to a shear stress which is independent of system size.

To test the predictions Eqs. (12) and (13) we compile in Fig. 6 the critical forces F_f and F_s of systems with different dimensions of the simulation box L at fixed rupture energy $\varepsilon=0.01$ and area fractions $\phi=0.7$ and 0.82, respectively. The data supports that the point of solidification F_s indeed decreases as L^{-1}: the quantity $F_s L/8\varepsilon$ does not only take a constant value irrespective of system size (crosses in Fig. 6), but the numbers close to 2 and 5 for $\phi=0.7$ and 0.82, respectively, are also plausible estimates for the average number of capillary bridges that will be ruptured upon displacing a disk by one diameter with respect to its right and left neighbors.

In contrast to F_s, the threshold for fluidization F_f increases stronger than linearly with L^{-1} (stars in Fig. 6). Interestingly, however, our data indicate that the gap between F_f and F_s closes as the system size increases. In line with the predictions of [8] for sheared assemblies of wet frictionless spheres, the system might then approach a critical state where different members of an ensemble of systems show vastly different behavior. Unfortunately, the determination of the fluidization line takes much more computational efforts than solidification. The preparation of the arrested state requires a slow decrease of the external driving force, and the subsequent fluidization, or yielding, of the solidified disks a sufficiently slow increase of the external driving force.

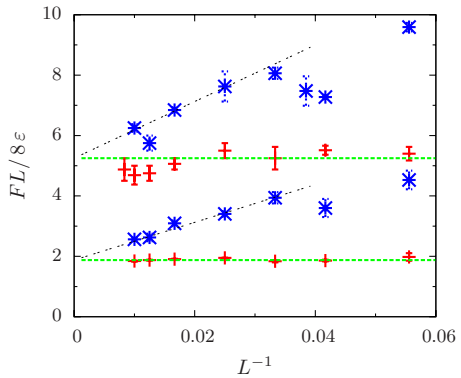

FIG. 6. (Color online) Amplitude of the external forces at solidification, $F_s L/8\varepsilon$ (+), and at fluidization, $F_f L/8\varepsilon$ (*), as function of the reciprocal system size L^{-1} for area fractions $\phi=0.7$ (lower lines) and $\phi=0.82$ (upper lines), respectively. The data for F_s are roughly constant, such that the values on the abscissa may be interpreted as the number of capillary bridges broken when displacing a disk by one diameter with respect to its neighbors to the left and right. The dashed line give the respective quadratic fits $LF_f/8\varepsilon \simeq 1.9+60/L$ and $LF_f/8\varepsilon \simeq 5.3+90/L$ for fluidization. The rupture energy is $\varepsilon=0.01$.

Hence, each of these data points takes more than one month of computational time. In addition, even the present data suffer from limited statistics due to strong history dependence of F_f. As a consequence, the calculation of accurate ensemble averages for the fluidization transition lies presently beyond reach of direct numerical integration.

E. Density dependence of critical forces

According to Fig. 6 the force required to keep the system in a fluidized state increases noticeably with the packing fraction of the disks. Indeed one would expect that the force diverges when approaching random close packing,

$$\frac{F_s L}{8\varepsilon} \sim \left(\frac{\phi_{\mathrm{rcp}}-\phi}{\phi}\right)^{-\alpha}, \tag{14}$$

where α is a positive exponent. In this expression the factor $1/(\phi_{\mathrm{rcp}}-\phi)$ can be interpreted as the smallest area where there is enough *free volume* for two disks to pass, and hence the ratio $\phi/(\phi_{\mathrm{rcp}}-\phi)$ amounts to the minimum number of disks that must be displaced in order to let two disks pass.

In order to explore this dependence we probe the critical forces for a range of packing fractions ϕ. For $\phi \gtrsim 0.84$ fluctuations in the drift velocity become so large that one cannot measure δv_y within reasonable error. This is not unexpected, however, since for the bidisperse system under consideration, $\phi_{\mathrm{rcp}}=0.84$ is the close-packing density reported in the literature, cf. [32,33].

For total area fractions $\phi \lesssim 0.5$, initially randomly distributed disks frequently condense into bands with arrested particle configurations that move in opposite directions. In this case the evolution of the system may follow entirely different scenarios: either the bands eventually collide and heat up. In this case, the system is attracted again to a stationary fluidized state. Alternatively, the bands may not touch. In that

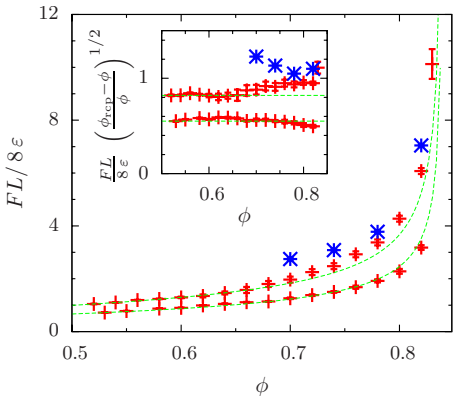

FIG. 7. (Color online) Amplitude of the external forces at solidification, $F_s L/8\varepsilon$ (+), and at fluidization, $F_f L/8\varepsilon$ (*), as function of the packing fraction ϕ, where the two curves for the solidification refer to rupture energy $\varepsilon=0.01$ (top) and $\varepsilon=0.05$ (bottom), respectively. As expected the forces diverge when approaching random close packing, and a smaller number of capillary bridges rupture when rearranging a system with a larger ε. The green dashed lines indicate that the forces diverge like a reverse square root of the nondimensionalized packing fraction $(\phi_{rcp}-\phi)/\phi$. To underline this assertion the inset shows that $F_s L[(\phi_{rcp}-\phi)/\phi]^{1/2}/8\varepsilon$ takes roughly constant values. The system size is $L=18$.

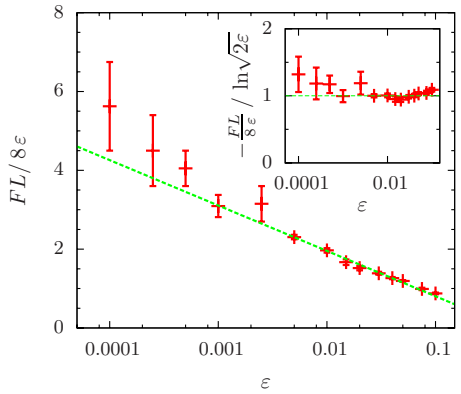

FIG. 8. (Color online) Amplitude of the external forces at solidification, $F_s L/8\varepsilon$ (+) as function of the rupture energy ε of capillary bridges. The dashed green line shows a logarithmic fit to the data: $FL/8\varepsilon \simeq -\ln\sqrt{2\varepsilon}$. The quality of the fit is again underlined by an inset demonstrating that $-F_s L/(8\varepsilon \ln\sqrt{2\varepsilon}) \simeq 1$. The area fraction of the disks is $\phi=0.7$, and $L=18$.

case, the system stays cool and the two bands persist. Consequently, in the present study we focus on area fractions $0.52 \leq \phi \leq 0.82$ where the system approaches a unique steady state irrespective of sample preparation.

In Fig. 7 we compile data for the critical forces as a function of ϕ. As anticipated, the force diverges when the close-packing density $\phi_{rcp}=0.84$ is approached. The exponent is found to be $\alpha \simeq 1/2$, as shown in the inset. This may be interpreted as stating that the passing of a pair of disks leads to collective displacements in a region containing $N_\phi^2 = \phi/(\phi_{rcp}-\phi)$ disks, and that the displacement goes along with a "micro-crack" where the capillary bridges between N_ϕ out of these N_ϕ^2 disks rupture.

F. Master plot for the critical force

The estimate Eq. (14) involves a prefactor which is a function of the rupture energy ε. Varying the rupture separation at fixed system size L and packing fraction ϕ suggests (cf. Fig. 8) that this prefactor might scale as $-\ln\sqrt{2\varepsilon}$. Forthcoming work will have to address the question whether this might be attributed to an exponential screening of stresses in the system. In addition, a full explanation of this dependence will then also have to take into account that the energy content of the solidified state increases upon increasing the rupture separation.

Irrespective of the physical origin of the dependence the scaling of $F_s L/8\varepsilon$ with ε allows us to write the critical force at the solidification transition as

$$F_s \simeq -B\,\frac{8\varepsilon}{L}\,\ln\sqrt{2\varepsilon}\left(\frac{\phi}{\phi_{rcp}-\phi}\right)^{1/2}, \qquad (15)$$

with a numerical prefactor $B=(0.45\pm0.05)$. That this expression fully covers the parameter dependence of F_s is demonstrated by a data collapse shown in Fig. 9 which contains all data shown so far.

IV. CONCLUSION AND OUTLOOK

In this paper, we studied the transition between a solidified and a fluidized state of a frictionless 2D wet granulate subjected to a shear force. To gain insight into the nature of this transition, we compared molecular-dynamics simulations of soft disks to theoretical estimates on the parameter dependence of the transition. In doing so, we concentrated on densities $\phi \gtrsim 0.52$ where the system remains spatially uniform and is free of persistent cracks and shear bands on the scale of the system size. In contrast to the majority of published works on sheared granulates, where Lees Edwards boundary

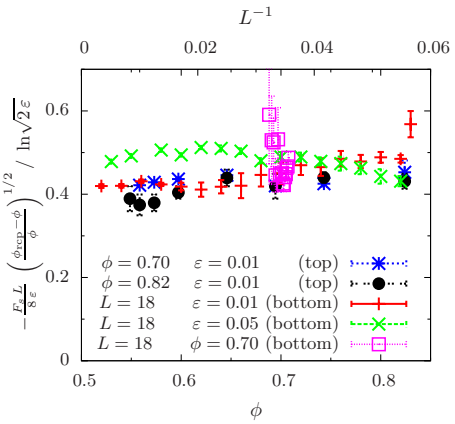

FIG. 9. (Color online) The plot compiles all data of the critical force at solidification, F_s, that are also shown in Figs. 6–8. The data collapse demonstrates that the force F_s is faithfully described by Eq. (15) with a proportionality constant of the order of 0.45. The parameters of the system are specified in the legend of the plot which also indicates whether the top or bottom axis is used as mantissa. Moreover, for better visibility the ϕ values of the last data set, where ε is varied, have slightly been displaced.

conditions are employed [15,34,35], the shear stress in the assembly is generated by means of a spatially varying body force acting on each disk. The stress induced by the body forcing is accumulated in a region close to the inflection point of the velocity profile, and the balance between dissipation due to rupture of capillary bridges on the one hand, and the acceleration by the external field on the other hand admits to derive analytical estimates for the smallest forcing still admitting a fluidized state.

The transition from the fluidized to the solidified state and back shows strong hysteresis. The critical force F_f required to fluidize a frozen state depends strongly on the history of the sample, as becomes apparent from a comparison of the force F_f obtained for packings prepared by different preparation protocols. In view of the prohibitively high requirements on computation time needed to determine the ensemble average which provides a precise yield point, so far only preliminary results could be reached on the parameter dependence of this point. However, these data indicate that there are two interesting limits where the hysteresis might disappear: (i) very large system size as shown in Fig. 6, and (ii) when approaching the close-packing limit shown in Fig. 7.

These findings are in marked contrast to the results reported on the 3D system [8,17], where no hysteresis was observed. That transition appeared instead to be continuous, and accompanied by strong (algebraically diverging) fluctuations. This calls for a renewed effort on the 3D system, including similar parameter variations and finite-size scaling as in the present work. This will be particularly interesting in view of a recent study [36] of a 3D granular system of purely repulsive soft-core particles with a fixed restitution coefficient. In that case the transition between the fluidized and solidified state shows hysteresis for all finite shear stresses, and inertia of the flow was identified as its origin.

In order to compare our results with findings on kinetic arrest of systems with conservative forces and/or collisions with a finite restitution coefficient, it is tempting to interpret the ratio T_g/ε of the granular temperature T_g over the energy ε, which characterizes the strength of capillary interactions, as a temperature-like variable in the spirit of [23]. This connects the transition investigated in the present paper to the gelation transition in colloidal systems [23,37], the glass transitions in systems with soft-core repulsive interactions [25,26], and to aggregation and jamming in dry fine powders [24]. The analogy appears to be valid to the extend that—just as in gels and coagulating powders—the capillary interaction in wet granulates leads to the formation of clusters of particles with a frozen contact network and stress propagation through the network. On the other hand, the reduced temperature T_g/ε is *not* a temperature-like variable in the spirit [26,37,38] of mode-coupling theory. The flow at the fluidization threshold of wet granulates results solely from the applied shear force, and due to the hysteretic nature of the capillary forces motion immediately arrests in the absence of the external forcing. In this respect the solidification of wet granulates is more reminiscent to jamming of dry granular matter at zero temperature [36]. We hold that the energy dissipated upon rupture of capillary bridges is an independent thermodynamic variable which is distinct from the three variables (density, shear stress, and temperature) suggested to govern the jamming phase diagram [11,23,25,38]. Forthcoming work will have to explore features of arrest in the resulting four-dimensional parameter space. One possibility might be to consider the arrest of motion of a wet granulate with soft-core repulsive interaction that sets an energy scale for the temperature. The data collapse established in the present study will be of pivotal importance to explore this multidimensional parameter space.

In the fluidized state the system appears to be ergodic. Irrespective of sample preparation, we observe the same steady state. Moreover, in terms of the control parameter FL and order parameter Δv_y the system shows the same subcritical solidification transition.

In appropriate dimensionless units the normalized critical force F_s at the solidification point is inversely proportional to the lateral dimension of the system L and the square root of the reduced number density $(\phi_{\mathrm{rcp}}-\phi)/\phi$ of the assembly of disks. In addition, there also is a weak (logarithmic) dependence on the rupture energy ε of the capillary bridges. We provide an explicit formula, Eq. (15), for these dependences, and underpin it with a data collapse Fig. 9.

The linear dependence of F_s on the reciprocal lateral dimension L^{-1} is ascribed to a balance of power input from the external field and dissipation due to rupture of capillary bridges. For its dependence on packing fraction we offer an explanation in terms of free volume in the system and the length of micro-cracks required to rearrange disks in the fluid state.

The uncovering of universal properties of the solidification transition is the most important finding of this communication. Together with the observed ergodicity in the fluidized state this strongly suggests the feasibility of a continuum theory of sheared assemblies of wet disks, similar to the hydrodynamic description of dense inelastic hard disks under shear as presented by Jenkins [39] and Khain [40]. It will be also interesting to discuss the appearance and stability of spatially-heterogeneous flow profiles in dense assemblies of wet disks which are driven by a cosine forcing [22] or Lees Edwards boundary conditions [34,40]. Forthcoming work will take up the challenge to build such a theory, and discuss its prospects and limitations for the description of phase transitions in granular systems.

ACKNOWLEDGMENTS

We are grateful to Johannes Blaschke, Ohle Claussen, Andrey Milchev, Klaus Röller, Matthias Schröter, and Sonia Utermann for valuable discussions.

[1] H. M. Jaeger, S. R. Nagel, and R. P. Behringer, Rev. Mod. Phys. **68**, 1259 (1996).
[2] P. A. Thompson and G. S. Grest, Phys. Rev. Lett. **67**, 1751 (1991).
[3] C. S. Campbell, J. Fluid Mech. **465**, 261 (2002).
[4] G. MiDi, Eur. Phys. J. E **14**, 341 (2004).
[5] L. Aarons and S. Sundaresan, Powder Technol. **169**, 10 (2006).
[6] T. Pöschel and T. Schwager, *Computational Granular Dynamics* (Springer, New York, 2005).
[7] D. J. Hornbaker, R. Albert, I. Albert, A.-L. Barabási, and P. Schiffer, Nature (London) **387**, 765 (1997).
[8] S. Herminghaus, Adv. Phys. **54**, 221 (2005).
[9] N. Mitarai and F. Nori, Adv. Phys. **55**, 1 (2006).
[10] T. Gröger, U. Tüzün, and D. M. Heyes, Powder Technol. **133**, 203 (2003).
[11] A. J. Liu and S. R. Nagel, Nature (London) **396**, 21 (1998) news and views.
[12] C. S. O'Hern, L. E. Silbert, A. J. Liu, and S. R. Nagel, Phys. Rev. E **68**, 011306 (2003).
[13] J. A. Drocco, M. B. Hastings, C. J. Olson Reichhardt, and C. Reichhardt, Phys. Rev. Lett. **95**, 088001 (2005).
[14] A. S. Keys, A. R. Abate, S. C. Glotzer, and D. J. Durian, Nat. Phys. **3**, 260 (2007).
[15] P. Olsson and S. Teitel, Phys. Rev. Lett. **99**, 178001 (2007).
[16] T. Hatano, Phys. Rev. E **79**, 050301(R) (2009).
[17] M. Schulz, B. M. Schulz, and S. Herminghaus, Phys. Rev. E **67**, 052301 (2003).
[18] A. Fingerle and S. Herminghaus, Phys. Rev. Lett. **97**, 078001 (2006).
[19] A. Fingerle and S. Herminghaus, Phys. Rev. E **77**, 011306 (2008).
[20] K. Huang, M. Sohaili, M. Schröter, and S. Herminghaus, Phys. Rev. E **79**, 010301(R) (2009).
[21] S. H. Ebrahimnazhad Rahbari, J. Vollmer, S. Herminghaus, and M. Brinkmann, EPL **87**, 14002 (2009).
[22] K. Roeller, J. Vollmer, and S. Herminghaus, Chaos **19**, 041106 (2009).
[23] V. Trappe, V. Prasad, L. Cipelletti, P. Segre, and D. A. Weitz, Nature (London) **411**, 772 (2001).
[24] J. M. Valverde, M. A. S. Quintanilla, and A. Castellanos, Phys. Rev. Lett. **92**, 258303 (2004).
[25] Z. Zhang, N. Xu, D. T. Chen, P. Yunker, A. M. Alsayed, K. B. Aptowicz, P. Habdas, A. J. Liu, S. R. Nagel, and A. G. Yodh, Nature (London) **459**, 230 (2009).
[26] L. Berthier and T. A. Witten, Phys. Rev. E **80**, 021502 (2009).
[27] C. D. Willett, M. J. Adams, S. A. Johnson, and J. P. K. Seville, Langmuir **16**, 9396 (2000).
[28] S. Nowak, A. Samadani, and A. Kudrolli, Nat. Phys. **1**, 50 (2005).
[29] M. Scheel, R. Seemann, M. Brinkmann, M. D. Michiel, A. Sheppard, B. Breidenbach, and S. Herminghaus, Nature Mater. **7**, 189 (2008).
[30] A. Fingerle, K. Roeller, K. Huang, and S. Herminghaus, New J. Phys. **10**, 053020 (2008).
[31] B. D. Lubachevsky and F. H. Stillinger, J. Stat. Phys. **60**, 561 (1990).
[32] N. Xu, C. S. O'Hern, and L. Kondic, Phys. Rev. Lett. **94**, 016001 (2005).
[33] N. Xu, Ph.D. thesis, Yale University, 2005.
[34] T. Hatano, J. Phys. Soc. Jpn. **77**, 123002 (2008).
[35] C. Heussinger and J.-L. Barrat, Phys. Rev. Lett. **102**, 218303 (2009).
[36] M. Pica Ciamarra and A. Coniglio, Phys. Rev. Lett. **103**, 235701 (2009).
[37] P. N. Segrè, V. Prasad, A. B. Schofield, and D. A. Weitz, Phys. Rev. Lett. **86**, 6042 (2001).
[38] M. P. Ciamarra, M. Nicodemi, and A. Coniglio, Soft Matter **6**, 2871 (2010).
[39] J. T. Jenkins, Phys. Fluids **18**, 103307 (2006).
[40] E. Khain, Phys. Rev. E **75**, 051310 (2007).
[41] We use the term *fluidized state* rather than *fluid* to stress the fact that the assembly of disks spontaneously transforms into an *arrested state* once the shear force is switched off.